RSC Advances

PAPER

View Article Online
View Journal | View Issue

Cite this: *RSC Adv.*, 2022, **12**, 21725

Co-pyrolysis characteristics and kinetics of low metamorphic coal and pine sawdust

Pei Zhang,[a] Zhaoyang Chen,[a] Qiuli Zhang, *[a] Shuo Zhang,[a] Xiaogang Ning[b] and Jun Zhou[a]

Co-pyrolysis experiments with low metamorphic coal (LC) and pine sawdust (PS) were carried out in a fixed-bed pyrolysis reactor. The effect of biomass addition on the yield distribution and composition of the coal pyrolysis products was investigated. The pyrolysis behavior was studied by thermogravimetric analysis. The Coats–Redfern integral and Achar differential methods were used to study the mechanism functions and the kinetic parameters of the pyrolysis process of each sample. The results show that there is a synergistic effect on the co-pyrolysis and it is most pronounced at a PS mixing ratio of 30%, and it results in improved tar and gas yields. Part of the polycyclic aromatic hydrocarbons (PAHs) in the co-pyrolysis tar are converted into phenolic substances with a simple structure, which improves the quality of the tar. At the same time, the alcohols and acids in the PS and LC react to generate a large number of esters. The addition of PS shifted the LC pyrolysis process towards the low temperature region, lowering the pyrolysis temperature of the coal sample and increasing the pyrolysis rate of the sample. The main pyrolysis process of LC conforms to the second-order chemical reaction law with an activation energy of 35.93 kJ mol^{-1}, and the main pyrolysis process of PS conforms to the one-dimensional diffusion parabolic law with an activation energy of 63.84 kJ mol^{-1}, and the main pyrolysis process of LC and PS co-pyrolysis conforms to a second-order chemical reaction law with an activation energy of 86.19 kJ mol^{-1}.

Received 17th April 2022
Accepted 17th July 2022

DOI: 10.1039/d2ra02461f

rsc.li/rsc-advances

Introduction

The domestic energy structure has exhibited the characteristics of "lack of oil and gas, sufficient coal". The low-metamorphic coal (LC) in northern Shaanxi has a high tar content and large reserves. Its utilization process mainly adopts the pyrolysis process to produce tar, gas and semi-coke.[1] Increasing the yield and quality of pyrolysis tar can effectively alleviate the increasing shortage of domestic oil resources. Biomass resources are abundant, renewable, recyclable and highly reactive.[2] Taking advantage of its high hydrogen : carbon ratio[3] can make up for the disadvantage of low hydrogen content in coal.[4] By co-pyrolyzing LC with biomass, on the one hand, the presence of coal can compensate for the low calorific value and low density of the biomass, and on the other hand biomass as a hydrogen donor in the co-pyrolysis process can improve the yield of the coal pyrolysis tar.[5] Therefore, studying co-pyrolysis can provide a flexible solution for energy and chemical feedstock supply.[6]

Several researchers have studied the co-pyrolysis process of coal and different types of biomass and found that there is a certain synergistic effect in co-pyrolysis,[7–9] and the mixing ratio of biomass, temperature, and heating rate all have varying degrees of influence on the product distribution and synergistic effect.[10,11] Zhao *et al.*[12] co-pyrolyzed crop straw and lignite, and found that the heat generated by the co-pyrolysis reaction can further accelerate the pyrolysis of the lignite. Zhao *et al.*[13] performed co-pyrolysis of lignite with crop straw and found that co-pyrolysis produced significant synergistic effects on the yield and composition of tar, semi-coke and gas. Wu *et al.*[14] conducted co-pyrolysis of low-rank coal and biomass, and found that the synergistic effect of vitrinite of low-rank coal on volatile oil yield is closely related to its mass ratio, and inertinite inhibits the formation of volatiles during co-pyrolysis. Huang *et al.*[15] found synergistic effects of bituminous coal and biomass co-pyrolysis, especially at a bituminous coal to biomass mixing ratio of 70 : 30 and a temperature of 600 °C. Guo and Bi[16] co-pyrolyzed sub-bituminous coal with corn straw and found that with an increase of the corn straw ratio and the temperature, the yield of gas and tar increased, and more light oil and water was found during co-pyrolysis.

A pyrolysis kinetic model is an important tool for gaining insight into co-pyrolysis mechanisms, to improve pyrolysis

[a]*School of Chemistry and Chemical Engineering, Xi'an University of Architecture and Technology, Xi'an 710015, China. E-mail: qiulizhang@126.com*
[b]*Shaanxi Beiyuan Chemical Industry Group Co., Ltd, Jinjie Industrial Park, Shenmu 719319, Shaanxi, China*

technology and design of pyrolysis reactors.[17,18] Many researchers have explored the co-pyrolysis reaction using thermodynamic methods. At present, the methods used to study the kinetics mainly include the Coats–Redfern (CR) method, the general integration method, the Flynn–Wall–Ozawa (FWO) method, the Kissinger method, the MacCallum–Tanner method and so on.[19–21] Florentino-Madiedo *et al.*[22] used Criado and CR methods to elucidate the reaction mechanism of the pyrolysis process of coal, torrefied sawdust, paraffin and their blends. Ali *et al.*[23] used the thermodynamic method of CR to determine the kinetic decomposition parameters of wood. Ma *et al.*[24] used the Redfern model to obtain the kinetic parameters of cow dung (CM) and Meihuajing bituminous coal (MHJ), and found that the activation energy increased with the addition of CM. Using CR and FWO methods, Zhu *et al.*[25] found that the activation energy and reaction order of co-pyrolysis of bio-oil distillation residue and bituminous coal increased with the increase of the bituminous coal blending ratio. Domestic coal is widely distributed and there are different types, and the structure and composition of coal in different regions are quite different. However, the LC reserves in northern Shaanxi are large and the oil content is high, but not much research on co-pyrolysis of coal in northern Shaanxi and biomass has been done. The kinetic mechanism of co-pyrolysis is also unclear, so it is necessary to study its co-pyrolysis, and to achieve the improvement of the yield and quality of coal pyrolysis tar.

In research reported in this paper, the co-pyrolysis characteristics and kinetic characteristics of coal and biomass were studied, and the distribution of co-pyrolysis products under different mixing ratios of PS was studied. The mechanism function and kinetic parameters of the pyrolysis process were investigated by the CR integral method and the Achar differential method. The results of the research provide a theoretical basis for further understanding of the pyrolysis mechanism, product regulation and equipment development for the co-pyrolysis of coal and biomass.[26]

Experimental

Materials

The raw materials used in this study were LC and woody biomass PS, and the LC came from a chemical plant in Northern Shaanxi and the PS came from a feed plant in Northern Shaanxi. The proximate analysis and ultimate analysis results of both are shown in Table 1.

Experimental device and method

The experimental device for the pyrolysis is shown in Fig. 1, and the pyrolysis experiment was carried out using a tube furnace reactor. The LC and PS with particle sizes of less than 75 μm were mixed uniformly. The total mass was 50 g and the mixing ratios of the PS were 0%, 10%, 20%, 30%, 40%, 50%, and 100%. The sample was put into a quartz tube, and before heating, nitrogen (N_2) was introduced for 30 min to expel the air in the reactor and the airtightness of the device was checked. Then it was heated from room temperature to 675 °C at a heating rate of 10 °C min^{-1} and then held at a constant temperature for 30 min. The pyrolysis liquid products (pyrolysis water and tar) were collected by condensation in an air cooling bottle, and primary and secondary water-cooled bottles. After removing the water, the tar components were qualitatively and quantitatively analyzed by gas chromatography-mass spectrometry (GC-MS, ThermoScientific ISQ 7000). The obtained mass spectrum was compared with the NIST library database to identify the composition of the tar, and the peak area normalization method was used to determine the content of each component of the tar. The pyrolysis gas product was collected using a gas collection bag after passing the gas through a drying bottle, and a portable gas analyzer was used to measure the gas composition and content. Finally, the semi coke mass was weighed. The yield calculation for semi-coke, tar and gas of pyrolysis products is as follows:

$$Y_{\text{char}} = \frac{m_{\text{char}} - mA_{\text{ad}}}{m(1 - M_{\text{ad}} - A_{\text{ad}})} \times 100\% \quad (1)$$

$$Y_{\text{tar}} = \frac{m_{\text{tar}}}{m(1 - M_{\text{ad}} - A_{\text{ad}})} \times 100\% \quad (2)$$

$$Y_{\text{gas}} = 1 - Y_{\text{char}} - Y_{\text{tar}} \quad (3)$$

where Y_{char} is the semi-coke yield (%) m_{char} is the semi-coke mass (g), m is the mixed feedstock mass (g), and A_{ad} is the ash content (%), M_{ad} is the moisture content (%), Y_{tar} is the tar yield (%), m_{tar} is the tar mass (g), and Y_{gas} is the gas yield (%).

The theoretical yield of co-pyrolysis is calculated using eqn (4):

$$w_{\text{cal}} = (a \times w_{\text{coal}}) + (b \times w_{\text{bio}}) \quad (4)$$

$$\Delta w = w_{\text{exp}} - w_{\text{cal}} \quad (5)$$

where w_{cal} is the theoretical yield (%), w_{coal} is the yield of the coal pyrolysis products (%), w_{bio} is the yield of biomass pyrolysis products (%), a is the mass fraction of coal (%), b is the mass fraction of biomass (%), w_{exp} is the actual yield (%), and Δw is the difference between the experimental and theoretical values.

Table 1 Industrial analysis and elemental analysis of low metamorphic coal and pine sawdust

	Proximate analysis (wt%, air-dried basis)				Ultimate analysis (w%, dry ash-free basis)				
	Moisture	Ash	Volatile matter	Fixed carbon	C	H	O	N	S
PS	8.7	1.51	83.17	6.62	46.3	6.52	47.05	0.1	0.03
LC	18.08	4.96	33.35	43.62	80.1	4.05	14.28	1.09	0.51

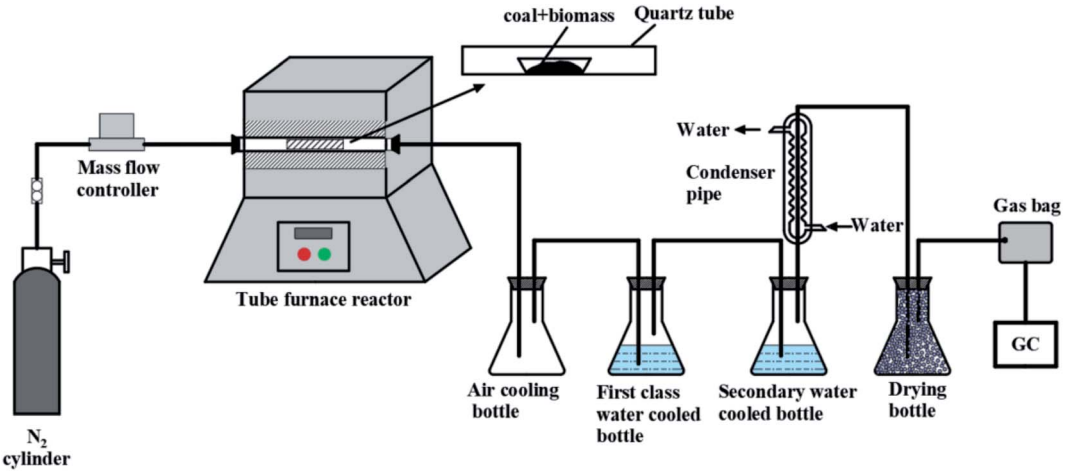

Fig. 1 Connection diagram of the pyrolysis experimental device.

Thermogravimetric analysis (TG)

Using a thermogravimetric analysis (TGA), samples weighing approximately 10 ± 0.1 mg were transferred to a platinum crucible under a N_2 atmosphere at a flow rate of 50 cm^3 min^{-1} and heated from room temperature to 875 °C at a rate of 10 °C min^{-1} for the TGA.

Kinetic analysis of the pyrolysis processes

There have been a lot of studies on the kinetic model of the co-pyrolysis of coal and biomass, among which the CR method is widely used. This method treats the solid reaction as a single reaction, and the calculated activation energy has a large error. In order to reduce the calculation error, in this study both the CR integral equation and the Achar differential equation are applied to the TG data for kinetic analysis, to determine the most probable mechanism function of the pyrolysis process, and to calculate the kinetic parameters of the pyrolysis process.[27,28] The specific calculation formula is given next.

The CR integral equation:

$$G(\alpha) \cong \frac{A}{\beta}\frac{RT^2}{E}\left(1-\frac{2RT}{E}\right)\exp\left(-\frac{E}{RT}\right) \quad (6)$$

$$\ln\left[\frac{G(\alpha)}{T^2}\right] = \ln\left(\frac{AR}{\beta E}\right)\left(1-\frac{2RT}{E}\right) - \frac{E}{RT} \quad (7)$$

For most reactions, $2RT/E \ll 1$, therefore eqn (6) can be simplified to:

$$\ln\left[\frac{G(\alpha)}{T^2}\right] = \ln\left(\frac{AR}{\beta E}\right) - \frac{E}{RT} \quad (8)$$

The Achar differential equation:

$$\ln\frac{\mathrm{d}\alpha}{f(\alpha)\mathrm{d}T} = \ln\frac{A}{\beta} - \frac{E}{RT} \quad (9)$$

where, α is the conversion function, A is the pre-exponential factor, E is the activation energy, R is the universal gas

Table 2 Commonly used solid phase decomposition reaction mechanism functions

Reaction class	Mechanism	Symbol	$f(\alpha)$	$G(\alpha)$
Random nucleation and nuclei growth	Two-dimensional	A2	$2(1-\alpha)[-\ln(1-\alpha)]^{1/2}$	$[-\ln(1-\alpha)]^{1/2}$
	Three-dimensional	A3	$3(1-\alpha)[-\ln(1-\alpha)]^{2/3}$	$[-\ln(1-\alpha)]^{1/3}$
Diffusion	One-dimensional	D1	$1/(2\alpha)$	α^2
	Two-dimensional	D2	$[-\ln(1-\alpha)]^{-1}$	$\alpha + (1-\alpha)\ln(1-\alpha)$
	Three-dimensional (Jander equation)	D3	$3/2(1-\alpha)^{2/3}[1-(1-\alpha)^{1/3}]^{-1}$	$[1-(1-\alpha)^{1/3}]^2$
	Three-dimensional (G-B equation)	D4	$3/2[(1-\alpha)^{-1/3}-1]^{-1}$	$1-2\alpha/3-(1-\alpha)^{2/3}$
Order reaction	First-order	F1	$1-\alpha$	$-\ln(1-\alpha)$
	Second-order	F2	$(1-\alpha)^2$	$(1-\alpha)^{-1}-1$
	Third-order	F3	$(1-\alpha)^3$	$[(1-\alpha)^{-2}-2]/2$
Exponential nucleation	Power law, $(n = 1/2)$	P2	$2\alpha^{1/2}$	$\alpha^{1/2}$
	Power law, $(n = 1/3)$	P3	$3\alpha^{2/3}$	$\alpha^{1/3}$
	Power law, $(n = 1/4)$	P4	$4\alpha^{3/4}$	$\alpha^{1/4}$
Phase boundary controlled reaction	One-dimensional movement	R1	1	α
	Contracting area	R2	$2(1-\alpha)^{1/2}$	$1-(1-\alpha)^{1/2}$
	Contracting volume	R3	$3(1-\alpha)^{2/3}$	$1-(1-\alpha)^{1/3}$

constant, T is the reaction temperature, β is the heating rate, $G(\alpha)$ is an integral function, and $f(\alpha)$ is a differential function.

Combined with Table 2, the $\ln[G(\alpha)/T^2]$ and $\ln[(d\alpha/dt)/f(\alpha)]$ in eqn (8) and (9) were curve-fitted to $1/T$. The values of E and A were obtained from the slope and intercept of the fitted straight line. The kinetic mechanism was determined according to a set of $f(\alpha)$ and $G(\alpha)$ with the closest activation energy, and R^2 was in the range of 0.95–0.99.

Results and discussion

Pyrolysis product yield distribution

The yield distributions of the pyrolysis products of each sample under different PS mixing ratios are shown in Fig. 2. The pyrolysis product of LC contained 5.8% tar and 2.66% gas, and the pyrolysis product of PS contained 21.26% tar and 11.65% gas. The tar and gas yield of PS was obviously higher than that of LC, whereas the semi-coke yield of LC was higher than that of PS. This is because LC is a PAH compound bonded by a strong C=C bond, whereas PS is a large polymer crosslinked by a weaker ether bond, which is more likely to break during pyrolysis,[29] so the volatile content of the PS pyrolysis was higher than that of LC. This corresponds to the volatile contents given in Table 1.

As shown in Fig. 2(a), the tar yield increased from 11.58% to 16.62% as the blending ratio of PS increased from 10% to 50%. Pine is a hydrogen-rich substance and many hydrogen-containing free radical fragments released during the pyrolysis process can interact with the macromolecular aromatic hydrocarbons in coal to promote its pyrolysis. At the same time, the high H/C ratio can prevent the free radical fragments which occurred during pyrolysis from undergoing condensation reactions or secondary reactions with the semi-coke. Therefore, the addition of PS facilitated the production of tar. As shown in Fig. 2(b), when the mixing ratio was increased from 10% to 50%, the gas production first increased and then decreased. The addition of PS favored the gas production which reached a maximum at 30% PS.

The difference between the experimental and theoretical values of the co-pyrolysis product yields for different mixing ratios is shown in Table 3. There were obvious deviations between the experimental and theoretical values of the three product yields. The experimental values of tar and gas were greater than the theoretical values, whereas the semi-coke was the opposite, indicating that there was a certain synergy in the co-pyrolysis process and that the synergy contributed to the production of tar and gas. The difference

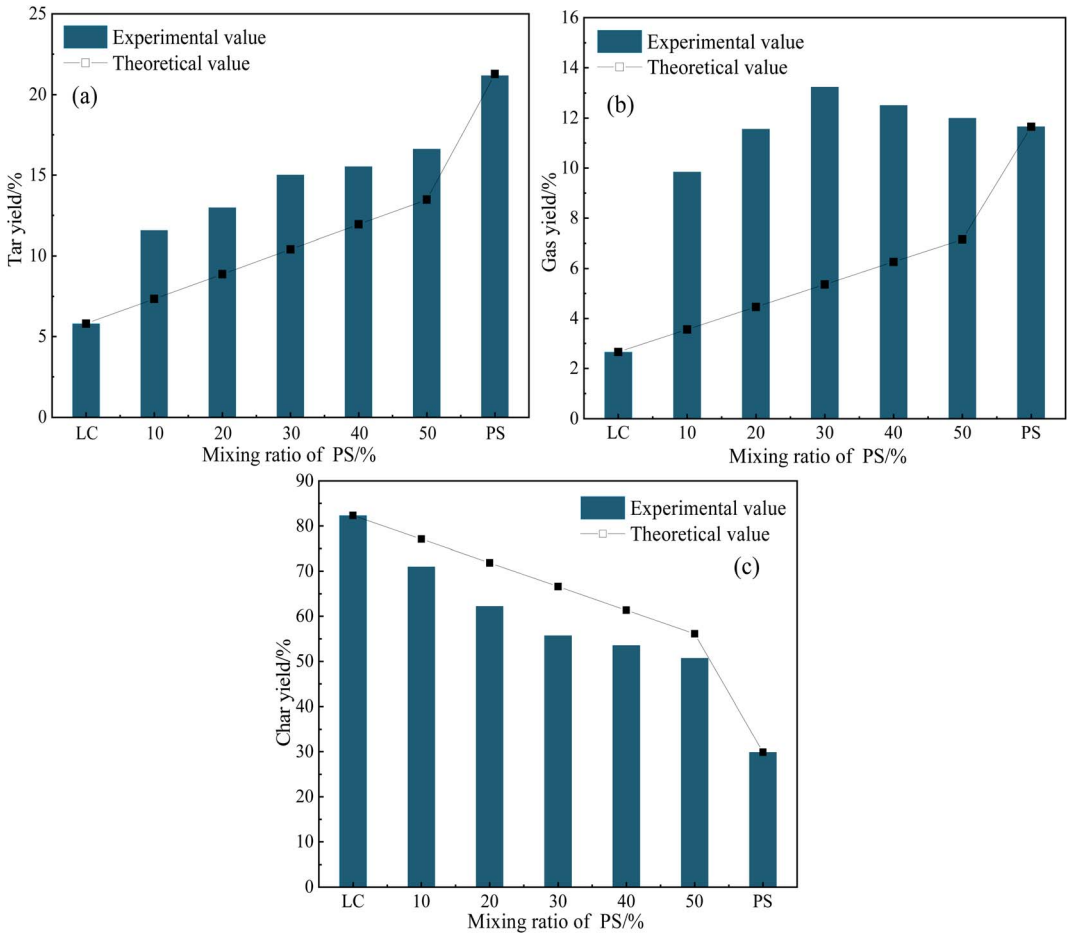

Fig. 2 The yield distributions of the pyrolysis products (a) tart, (b) gas and (c) char, with different mixing ratios of PS.

Table 3 The difference between experimental value and theoretical value of co-pyrolysis product yield under different PS mixing ratios

	ΔW (%)				
Product	PS = 10%	PS = 20%	PS = 30%	PS = 40%	PS = 50%
Tar	4.244	4.108	4.612	3.586	3.14
Gas	6.281	7.102	7.883	6.254	5.275
Char	−6.12	−9.59	−10.87	−7.81	−6.43

between the actual and theoretical values of each product was greatest when the PS mixing ratio was 30%. Therefore, the synergistic effect was most pronounced at a PS mixing ratio of 30%.

The GC-MS analysis of tar

According to previous research results, the synergistic effect was most obvious when the mixing ratio of PS was 30%.

Therefore, the co-pyrolysis tar with the mixing ratio of 30% was studied experimentally. The tars generated by LC, LC+30% PS and PS were analyzed by GC-MS, and the mass spectra obtained are shown in Fig. 3. Each peak was qualitatively and quantitatively analyzed, and all the substances were classified and counted. The results are shown in Fig. 4.

The composition analysis of the pyrolysis tar of LC is shown in Fig. 4(a). The highest content of aromatic hydrocarbons and alkanes in the tar was 21.22% and 27.39%, respectively, followed by phenols and esters with 9.5% and 13.13%, respectively. This is due to the fact that the structure of LC was dominated by polymeric aromatic polymers, which include a relatively high number of cyclic structures as well as alkyl side chains,[30] but a relatively low number of less saturated olefin branched chains.

The composition analysis of the pyrolysis tar of PS is shown in Fig. 4(b). The highest contents of phenols and ketones in tar were 29.91% and 24.81%, respectively, followed by esters and aldehydes at 15.65% and 11.63%, respectively, whereas the content of aromatic hydrocarbons and alkanes was the lowest. The structure of PS was mainly composed of hemicellulose, cellulose and lignin, which were high in oxygen content and therefore more conducive to the production of oxygenated substances such as phenols, esters, ketones, aldehydes and acids.[31]

The analysis of co-pyrolysis tar components is shown in Fig. 4(c). Compared with LC pyrolysis, the contents of phenols and esters in the co-pyrolysis tar components were 39.07% and 27.11%, respectively, which was a significant increased, which accounted for the main components of co-pyrolysis tar. The relative contents of aromatic hydrocarbons, alkanes and olefins decreased significantly. A comparison of the experimental and theoretical values showed that the experimental values for phenolics and esters were much larger than the theoretical values, which indicated that there was an obvious, positive synergistic effect of co-pyrolysis on these two substances, whereas the actual values for hydrocarbons and alcohols were smaller than the theoretical values, and the experimental values for other oxygenated compounds did not differ much from the theoretical values.

The area percentage of aromatic components in the pyrolysis tar of each sample is shown in Table 4. Compared to the LC pyrolysis alone, the content of naphthalene, anthracene and phenanthrene PAHs in the co-pyrolysis tar decreased, whereas

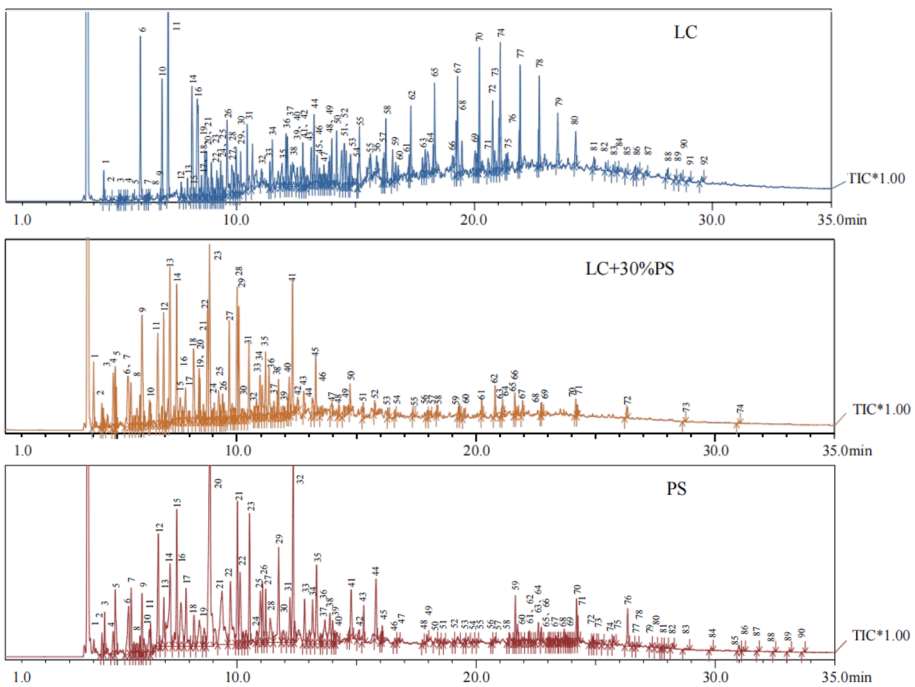

Fig. 3 The GC-MS profiles of each sample.

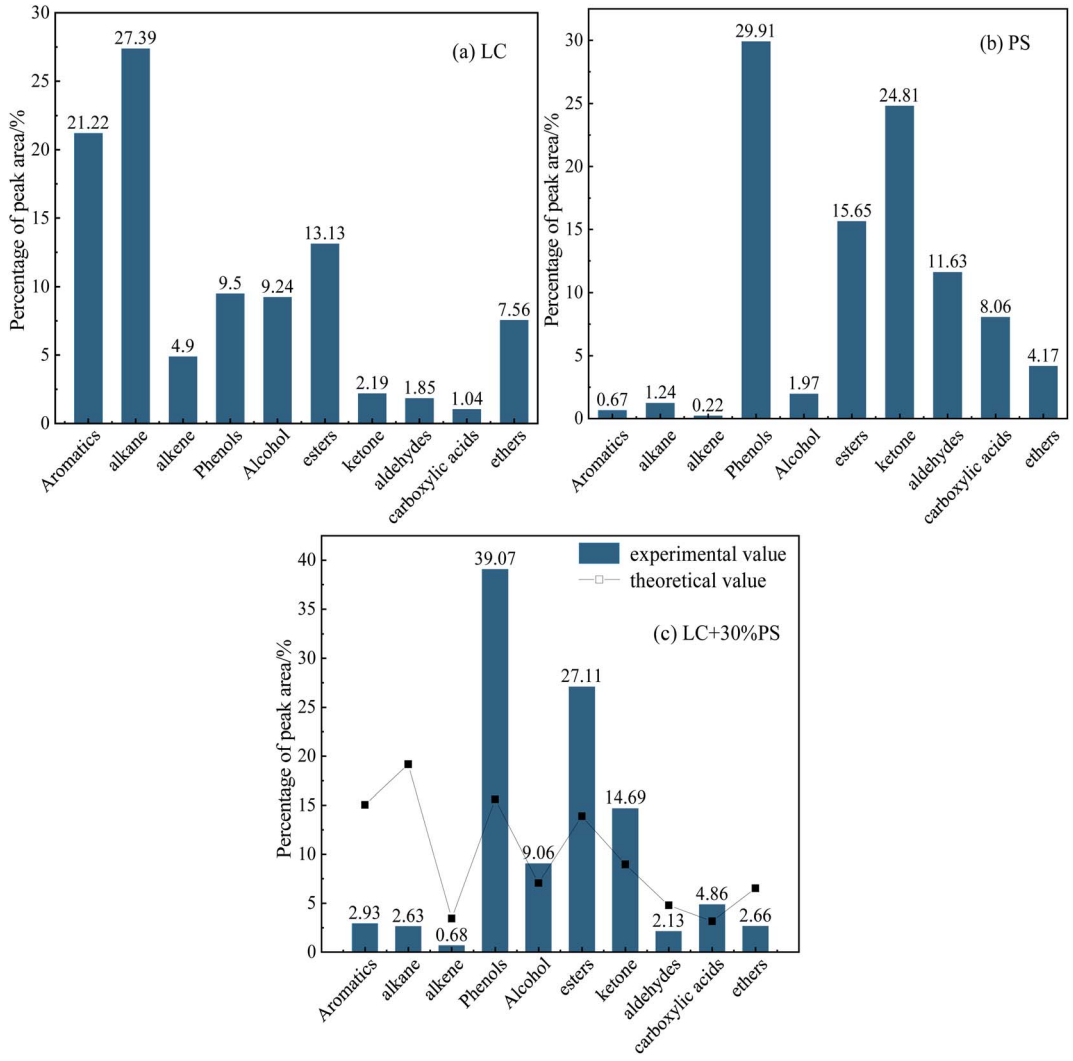

Fig. 4 The relative content of pyrolysis tar components in each sample.

the phenolics in the co-pyrolysis tar increased significantly, and almost all of them were simple monocyclic phenolics as shown in Table 5. Therefore, the addition of PS converted some of the PAHs in the coal tar to simpler phenolics, thus, improving the quality of the tar. It was noted that this was similar to the conclusion of Huang *et al.*,[15] who showed that co-pyrolysis had a significant synergistic effect on the phenolic substances in tar components, which was conducive to the production of phenolic substances with a simple structure. The PS pyrolysis generated a large number of hydrogen and hydroxyl radicals that attacked the aromatic ring in the coal, whereas small amounts of alkali metals in the biomass can promote substitution reactions in the aromatic hydrocarbons, resulting in the formation of phenolics. Possible reactions are shown in eqn (10)–(16).

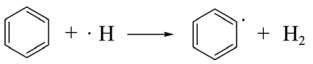

(10)

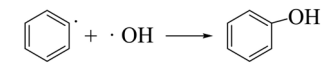

(11)

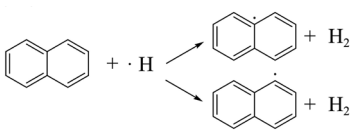

(12)

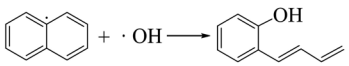

(13)

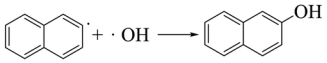

(14)

Table 4 Percentage areas of aromatic components in the pyrolysis tar of each sample (%)

	Benzenes	Naphthalenes	Anthracenes	Phenanthrenes	Pyrenes
LC	0.7937	12.2064	3.2878	1.9181	0.9605
LC+30%PS	—	1.3765	0.283	0.7436	—
PS	—	—	—	0.1386	0.2797

Table 5 The phenolic compounds in the pyrolysis tar of LC+30%PS

Compound	Structure	Compound	Structure
Phenol, 2-methoxy-4-(1*Z*)-1-propen-1-yl-		4-Methoxy-3-(methoxymethyl)phenol	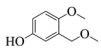
2-Isopropoxyphenol		3-Methoxy-2-benzenediol	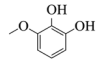
2-Methoxy-3-methylphenol		Phenol,3,4,5-trimethyl-	
Phenol, 2-ethoxy-4-methyl-		1,2,3-Benzenetriol,5-(1,1-dimethylethyl)-	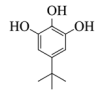
2,6-Dimethylphenol		Phenol,3-ethyl-5-methyl-	
1,2-Benzenediol,4-ethyl-		5-Benzofuranol	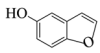
2,3-Dimethylhydroquinone			

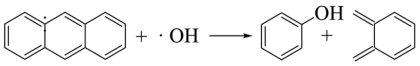

(15)

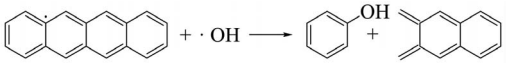

(16)

The relative contents of various esters in the pyrolysis tar of each sample are shown in Table 6. The esters in the co-pyrolysis tar were mainly aromatic esters, probably because the acetyl functional group on the hemicellulose breaks during the pyrolysis of PS, which in turn replaces the hydrogen atom on the phenolic hydroxyl group in the LC pyrolysis tar to produce esters, and the reaction for this is as shown in eqn (17). The alcohols and acids in PS and LC also react to form some esters, as shown in eqn (18)–(20). From Table 6 it can also be found that cyclic esters are produced in the co-pyrolysis tar that are not even present in the individual pyrolysis, where presumably cyclisation reactions such as eqn (21) occur.

Table 6 The relative content of various esters in different samples/%

	Aromatic esters	Fatty esters	Cyclic ester
LC	10.87	3.57	—
LC+30%PS	20.69	3.39	3.14
PS	11.45	1.14	—

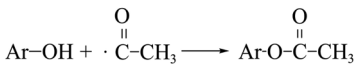

(17)

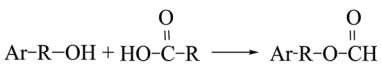

(18)

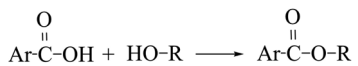

(19)

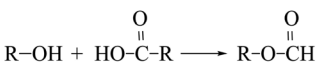

(20)

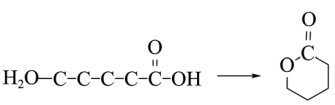

(21)

Gas composition analysis

The composition of the gas products at different PS mixing ratios is shown in Fig. 5. The gaseous products consist mainly of

CO_2, CO, CH_4, and H_2. As the PS blending ratio increased from 10% to 50%, the volume fraction of CO increased from 24.62% to 42.27%, whereas the volume fractions of CO_2 and C_nH_m remained basically unchanged. The PS structure was rich in oxygen-containing functional groups, such as –COOH and –C=O, which will break during pyrolysis to give more CO and CO_2,[32] and some of the CO_2 will react with the semi-coke to generate CO,[33] resulting in an increase in the content of CO. The decrease in the volume fraction of CH_4 from 18.42% to 7.71% was due to the fact that there were more ways to generate methane from LC pyrolysis, such as from fatty side chain breakage, from methyl or methylene breakage hydrogenation, and from saturated hydrocarbon cleavage above C_2[9]. Because the PS pyrolysis produced CH_4 mainly from the thermal decomposition of lignin, which was relatively small in content, so as the mixing ratio of PS increases, the CH_4 yield decreases.

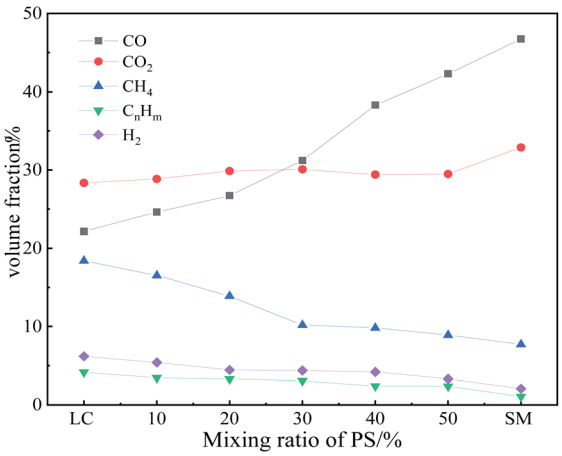

Fig. 5 The composition of the gas product at different mixing ratios of PS.

Determination of pyrolysis characteristics

The LC, PS, LC+30%PS were pyrolyzed using a TGA at a heating rate of 10 °C min^{-1}. The TG and derivative thermogravimetry (DTG) change curves are shown in Fig. 6.

According to the DTG curve, the pyrolysis process of each sample was divided into three stages, namely drying and degassing stage (I), main pyrolysis stage (II), and slow weight loss stage (III). The pyrolysis process of LC is shown in Fig. 6(a). The stage I of the LC pyrolysis process was from room temperature to 150 °C. This stage was mainly for the removal of moisture and surface adsorbates from the coal samples. The stage II was 350–600 °C and corresponded to the DTG curve with a weight loss peak at 451 °C, This stage was dominated by depolymerization and splitting reactions, where the side chain

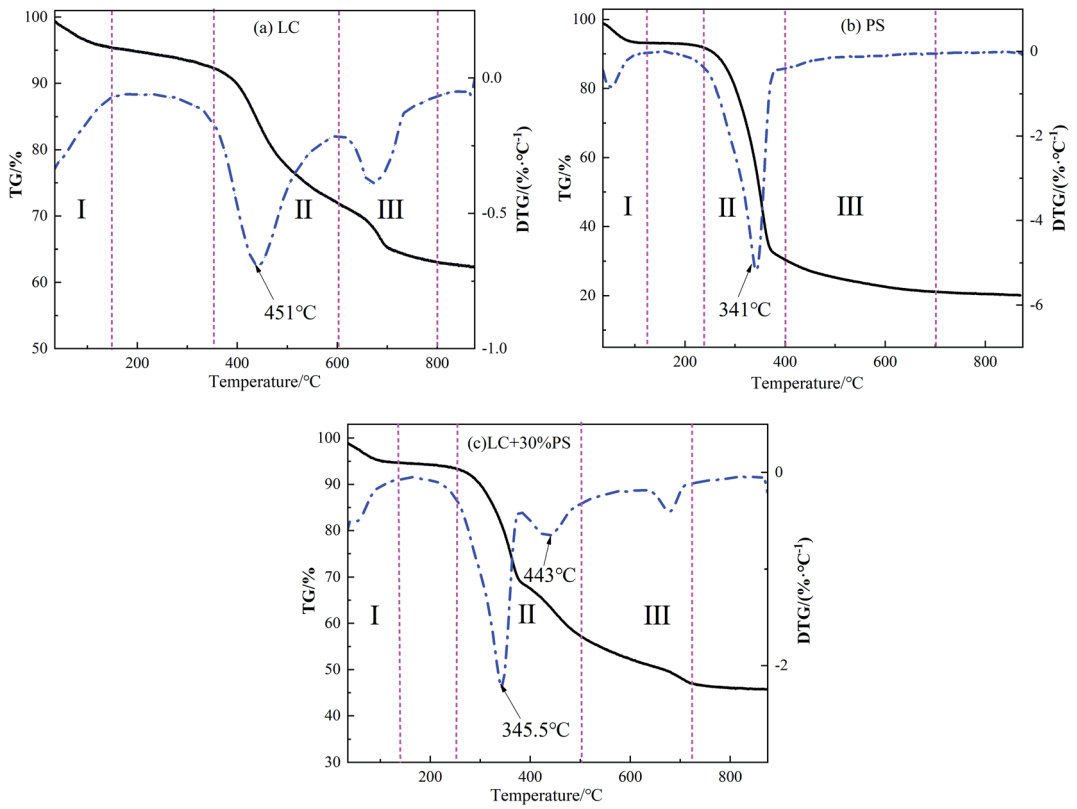

Fig. 6 The TG/DTG curves of each sample.

functional groups in the LC were thermally decomposed to produce large amounts of volatile hydrocarbons, mainly tar and pyrolysis gas. The stage III occurred at 600–800 °C, which corresponded to a small peak on the DTG curve. This stage is a secondary reaction stage where the semi-coke polycondensation generates coke while producing some H_2, CH_4 and other gases.[34] The pyrolysis process of PS is shown in Fig. 6(b). The stage I of PS pyrolysis was from room temperature to 120 °C, which was mainly drying and degassing. The stage II was at 230–400 °C, and the corresponding DTG curve shows a weight loss peak at 341 °C. In this stage, the pyrolysis reaction of hemicellulose and cellulose occurred.[35] Stage III was at 400–700 °C, where the more thermally stable lignin underwent pyrolysis reactions and the TG curve was relatively flat.

The co-pyrolysis process of LC+30% PS is shown in Fig. 6(c). Stage I was room temperature to 130 °C, and was consistent with the separate pyrolysis of PS and LC, and was dominated by the volatilization of water. Stage II was at 250–500 °C. Two weight loss peaks appeared on the DTG curve at this stage, with peaks of 345.5 °C and 443 °C, which corresponded to PS and LC pyrolysis, respectively. Stage III was at 500–720 °C and corresponded to a small peak on the DTG curve, which was most likely the secondary reaction stage of the LC.

The characteristic pyrolysis parameters of LC, PS and LC+30%PS are shown in Table 7, where T_{in} is the temperature at the beginning of the main pyrolysis stage, T_{max} is the temperature at the maximum weight loss rate, T_f is the temperature at the end of the main pyrolysis stage, $(\Delta m/t)_{max}$ is the maximum weight loss rate, and Δm is the final weight loss rate.

It can be seen from Table 7 that the main pyrolysis range of PS was 230–341 °C, and that of LC was 350–451 °C. When the PS reached the maximum pyrolysis rate, the LC started to pyrolyze. Therefore, the PS pyrolysis product acted as a hydrogen donor to promote the pyrolysis reaction of coal and generate more tar. The T_{in} and T_{max} of co-pyrolysis were at about 100 °C before those of LC, indicating that the addition of PS moved the LC pyrolysis process to the lower temperature region, and reduced the pyrolysis temperature of the coal samples. The $(\Delta m/\Delta t)_{max}$ of co-pyrolysis was significantly higher than that of LC, indicating that the addition of PS could also accelerate the pyrolysis rate of the coal samples.

Kinetic parameters

To further study the pyrolysis mechanism of coal, the kinetic calculation of the pyrolysis process of each sample was carried out. The solid phase decomposition reaction mechanism function of stage I is not discussed as stage I is mainly the removal of water and surface adsorbates. The activation energy, pre-exponential factor and the mechanism function to which the reaction process conforms were calculated for each sample in stages II and III at a heating rate of 10 °C min^{-1} and the results are shown in Table 8.

Table 8 shows that the activation energies of LC, PS and LC+30%PS are 24.12–35.93 kJ mol^{-1}, 60.23–86.19 kJ mol^{-1} and 55.76–63.84 kJ mol^{-1}, respectively. The activation energy of LC was lower than that of PS, and a low activation energy means high reactivity. The pre-exponential factor of PS was greater than that of LC. The larger the pre-exponential factor, the greater the reaction rate, which was consistent with the TGA results.

The kinetic mechanism of each sample was different at each pyrolysis stage, indicating that the reaction mechanism changed during the pyrolysis process. The main pyrolysis stage of LC conformed to the second-order chemical reaction law (F2), in which the bridge bond cleavage, fatty ester side chain cleavage and oxygen-containing functional group breakage mainly occurred, indicating that these reactions conform to the second-order chemical reaction law. The main pyrolysis stage of PS conformed to the one-dimensional diffusion parabola law (D1), and the pyrolysis reactions of hemicellulose and cellulose mainly occurred in this stage, indicating that these reactions conformed to the one-dimensional diffusion parabola law (D1). The reaction mechanisms of the main pyrolysis stages of LC and PS co-pyrolysis were consistent with LC and conformed to the second-order chemical reaction law (F2), indicating that the

Table 7 The characteristic pyrolysis parameters of each sample

Sample	T_{in} (°C)	T_{max} (°C)	T_f (°C)	$(\Delta m/\Delta t)_{max}$ (% min^{-1})	Δm (%)
LC	350	451	600	0.68	37.38
LC+30%PS	250	345	500	2.14	54.33
PS	230	341	400	5.13	79.95

Table 8 The kinetic pyrolysis parameters of each sample

Sample	Temperature range (°C)	E (kJ mol^{-1})	ln A	R^2	Mechanism	Mechanism symbol
LC	Stage II: 350–600	35.93	3.26	0.97322	Second-order	F2
	Stage III: 600–800	24.12	−2.20	0.95121	Three-dimensional (G-B equation)	D4
LC+30%PS	Stage II: 250–500	63.84	8.75	0.96343	Second-order	F2
	Stage III: 500–720	55.76	6.77	0.99594	Third-order	F3
PS	Stage II: 230–400	86.19	14.27	0.98621	One-dimensional	D1
	Stage III: 400–700	60.23	12.16	0.97492	Third-order	F3

pyrolysis mechanism of the co-pyrolysis process was mainly determined by the coal. In conclusion, the kinetic parameters provided an understanding of the reaction mechanism of the pyrolysis process and can also be used as a reference for industrial production.

Conclusions

The addition of PS to the LC contributed to the tar and gas production. As the mixing ratio of PS increased from 10% to 50%, the tar yield increased from 11.58% to 16.62%, and the gas yield increased from 9.84% to 12%. There is a synergistic effect of co-pyrolysis of LC and PS, and the synergistic effect is most obvious when the PS mixing ratio is 30%. Part of the polycyclic aromatic hydrocarbons in the co-pyrolysis tar are converted into phenolic substances with a simple structure, which improves the quality of the tar. At the same time, the alcohols and acids in PS and LC react to form a large number of esters. Therefore, a clear synergistic effect of phenols and esters appears. The addition of PS shifted the LC pyrolysis process towards the low temperature region, lowering the pyrolysis temperature of the coal sample and increasing the pyrolysis rate of the sample. The pyrolysis activation energy of LC is between 24.12 kJ mol^{-1} and 35.93 kJ mol^{-1}, and its main pyrolysis process conforms to the second-order chemical reaction law (F2). The pyrolysis activation energy of PS is between 60.23 kJ mol^{-1} and 86.19 kJ mol^{-1}, and its main pyrolysis process conforms to the one-dimensional diffusion parabola rule (D1). The co-pyrolysis activation energy of LC and PS is between 55.76 kJ mol^{-1} and 63.84 kJ mol^{-1}, and the main pyrolysis stage conforms to the second-order chemical reaction law (F2).

The results of the research reported in this paper provide a theoretical reference for the development of coal and biomass co-pyrolysis technology, and provide a flexible solution for improving the quality of tar and alleviating the shortage of petroleum resources.

Author contributions

Pei Zhang: conceptualization, methodology, writing–original draft. Qiuli Zhang: writing–review and editing. Zhaoyang Chen: formal analysis, software. Xiaogang Ning: investigation. Shuo Zhang: editing. Jun Zhou: supervision, administration.

Conflicts of interest

There are no conflicts to declare.

Acknowledgements

This work was supported by the National Natural Science Foundation of China (Grant No. 21663034), and the Innovation Capability Support Program of Shaanxi (Program No. 2020TD-028).

Notes and references

1 T. J. Morgan and R. Kandiyoti, *Chem. Rev.*, 2013, **114**, 1547–1607.
2 L. Cheng, Z. Q. Wu, Z. G. Zhang, C. Q. Guo, N. Ellis, X. T. Bi, A. P. Watkinson and J. R. Grace, *Appl. Energy*, 2020, **258**, 18.
3 P. B. Yang, S. H. Zhao, Q. G. Zhang, J. J. Hu, R. H. Liu, Z. Huang and Y. L. Gao, *Bioresour. Technol.*, 2021, **336**, 8.
4 J. Wei, M. Wang, F. Wang, X. Song, G. Yu, Y. Liu, H. Vuthaluru, J. Xu, Y. Xu and H. Zhang, *Int. J. Hydrogen Energy*, 2021, **46**, 17116–17132.
5 J. Wang, X. Liu, Q. Guo, J. Wei, X. Chen and G. Yu, *Fuel*, 2020, **268**, 117338.
6 Z. Q. Yang, Y. Q. Wu, Z. S. Zhang, H. Li, X. G. Li, R. I. Egorov, P. A. Strizhak and X. Gao, *Renewable Sustainable Energy Rev.*, 2019, **103**, 384–398.
7 X. F. Zhu, Y. M. Zhang, H. Z. Ding, L. R. Huang and X. F. Zhu, *Energy Convers. Manage.*, 2018, **168**, 178–187.
8 Z. Q. Wu, Y. W. Li, D. H. Xu and H. Y. Meng, *Fuel*, 2019, **236**, 43–54.
9 Z. Wu, W. Yang, Y. Li and B. Yang, *Bioresour. Technol.*, 2018, **255**, 238–245.
10 S. D. Li, X. L. Chen, A. B. Liu, L. Wang and G. S. Yu, *Bioresour. Technol.*, 2015, **179**, 414–420.
11 M. Ma, J. F. Wang, X. D. Song, W. G. Su, Y. H. Bai and G. S. Yu, *ACS Omega*, 2020, **5**, 16779–16788.
12 S. H. Zhao, P. B. Yang, X. F. Liu, Q. G. Zhang and J. J. Hu, *Bioresour. Technol.*, 2020, **302**, 8.
13 H. Y. Zhao, Q. Song, S. C. Liu, Y. H. Li, X. H. Wang and X. Q. Shu, *Energy Convers. Manage.*, 2018, **161**, 13–26.
14 Z. Q. Wu, J. Zhang, Y. J. Fan, B. Zhang, W. Guo, R. J. Zhang, Y. W. Li and B. L. Yang, *Fuel*, 2021, **306**, 16.
15 Y. Huang, N. B. Wang, Q. X. Liu, W. S. Wang and X. X. Ma, *Chin. J. Chem. Eng.*, 2019, **27**, 1666–1673.
16 M. Guo and J. C. Bi, *Fuel Process. Technol.*, 2015, **138**, 743–749.
17 H. J. Song, G. R. Liu, J. Z. Zhang and J. H. Wu, *Fuel Process. Technol.*, 2017, **156**, 454–460.
18 C. C. Geng, S. Y. Li, C. T. Yue and Y. Ma, *J. Energy Inst.*, 2016, **89**, 725–730.
19 R. K. Singh, T. Patil, D. Pandey, S. P. Tekade and A. N. Sawarkar, *J. Environ. Manage.*, 2022, **301**, 15.
20 B. B. Uzun and E. Yaman, *J. Energy Inst.*, 2017, **90**, 825–837.
21 K. V. Slyusarskiy, K. B. Larionov, V. I. Osipov, S. A. Yankovsky, V. E. Gubin and A. A. Gromov, *Fuel*, 2017, **191**, 383–392.
22 L. Florentino-Madiedo, M. F. Vega, E. Diaz-Faes and C. Barriocanal, *Fuel*, 2021, 292.
23 S. Ali, S. A. Hussain, M. Z. M. Tohir and A. A. Nuruddin, *Mater. Today: Proc.*, 2021, **42**, 178–185.
24 M. Ma, Y. H. Bai, X. D. Song, J. F. Wang, W. G. Su, M. Yao and G. S. Yu, *Sci. Total Environ.*, 2020, **728**, 9.
25 X. F. Zhu, K. Li, L. Q. Zhang, X. Wu and X. F. Zhu, *Energy Convers. Manage.*, 2017, **151**, 209–215.
26 N. Deparrois, P. Singh, K. G. Burra and A. K. Gupta, *Appl. Energy*, 2019, **246**, 1–10.

27 T.-S. Sun, Y.-M. Xiao, D.-Q. Wang, F.-L. Wang and Y.-T. Zhao, *Thermochim. Acta*, 1996, **287**, 299–310.
28 K. Muraishi, Y. Suzuki and A. Kikuchi, *Thermochim. Acta*, 1994, **239**, 51–59.
29 Z. He, Y. Sun, S. Cheng, Z. Jia, R. Tu, Y. Wu, X. Shen, F. Zhang, E. Jiang and X. Xu, *Fuel*, 2021, **287**, 119473.
30 S. Yi, X. M. He, H. T. Lin, H. Zheng, C. H. Li and C. Li, *Korean J. Chem. Eng.*, 2016, **33**, 2923–2929.
31 Z. Q. Wu, C. Ma, B. Zhang, J. Zhao, Z. Y. Xiao, M. Q. Li, H. Y. Meng, D. H. Xu and S. Z. Wang, *Energy Fuels*, 2020, **34**, 1111–1118.
32 T. T. Qu, W. J. Guo, L. H. Shen, J. Xiao and K. Zhao, *Ind. Eng. Chem. Res.*, 2011, **50**, 10424–10433.
33 F. S. Yang, A. N. Zhou, W. Zhao, Z. Y. Yang and H. J. Li, *Thermochim. Acta*, 2019, **673**, 26–33.
34 S. Li, J. Li and J. Xu, *Int. J. Hydrogen Energy*, 2021, **46**, 34652–34662.
35 H. J. Jeong, D. K. Seo, S. S. Park and J. Hwang, *J. Therm. Anal. Calorim.*, 2015, **120**, 1867–1875.